Applied Energy 300 (2021) 117394

Contents lists available at ScienceDirect

Applied Energy

journal homepage: www.elsevier.com/locate/apenergy

Harvesting energy from light and water droplets by covering photovoltaic cells with transparent polymers

L.E. Helseth

Department of Physics and Technology, Allegaten 55, 5020 Bergen, University of Bergen, Norway

HIGHLIGHTS

- Harvesting energy from light and water drops simultaneously using hidden or transparent front-electrode.
- Highest photovoltaic performance with surface charge transfer, lowest with electrostatic induction electrode.
- Curved electrodes allow easy removal of water drops.

GRAPHICAL ABSTRACT

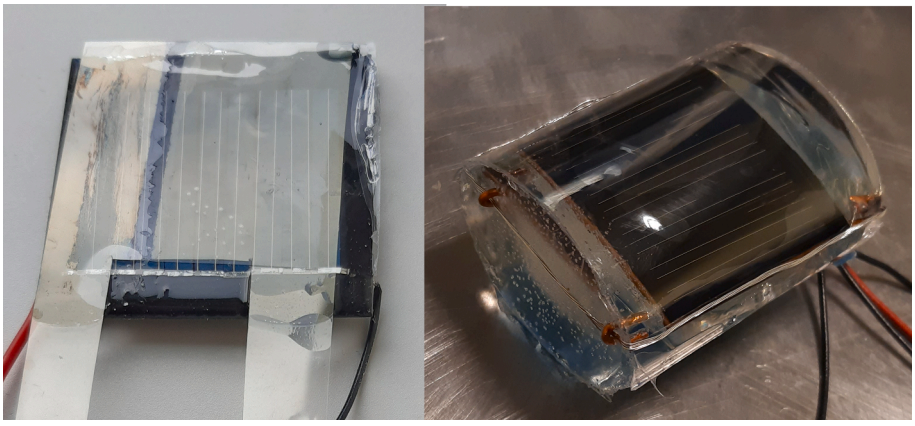

ARTICLE INFO

Keywords:
Photovoltaic cell
Contact electrification
Renewable energy

ABSTRACT

Energy harvesting of sunlight is often done using photovoltaic cells covered by a protective layer of polymer or glass. Currently, this layer does not have any other function than being transparent and protective, but its functionality could be improved and in fact contribute to electrical energy harvesting from the environment. This work reports new findings on the integration of silicon-based photovoltaic solar with a water droplet energy harvesting device based on contact electrification using readily available materials. The water droplet energy harvesting device utilizes hidden or transparent front electrodes in flat or curved geometries to increase the power output due to water droplets while at the same time minimizing the power loss from the photovoltaic cell. Three different designs are designed and tested, and the advantages and disadvantages are outlined. Particular emphasis is put on investigating the performance of the flat cell design that exhibited the largest electrical power output due to water droplet impact. The electrical energy harvesting efficiency of the commercial photovoltaic cell is about 4.4%, whereas for the water droplet energy harvesting device it is about 0.6%. The relative contributions of the two energy harvesting mechanisms are analyzed, and possible applications outlined.

1. Introduction

There is an increasing demand for local renewable electrical energy harvesting systems which do not need large scale investments or infrastructure. Photovoltaic solar cells are currently an important part of the strategy to fulfill these demands. However, an important question is

https://doi.org/10.1016/j.apenergy.2021.117394
Received 13 April 2021; Received in revised form 26 June 2021; Accepted 4 July 2021
Available online 15 July 2021

whether one could improve the energy harvesting by utilizing not only the sun light, but all the energy available from the environment. For example, in locations with rain, the associated kinetic energy should be harvested as well. Piezoelectric transducers have been considered for water droplet energy harvesting, with experiments dating back to 2008 [1]. Further investigations on cantilever systems [2,3] and water collection conditions [4], have revealed that the energy collecting electronics [5], the length of the cantilever [6] as well as its wetting properties [7] play important roles. However, the electrodes and interfaces are usually not transparent or may require moving parts which are not easily integrated into a photovoltaic solar cell. On the other hand, it has been demonstrated that triboelectric generators can integrated with photovoltaic cells. These contact electrification devices can be made by combining transparent electrodes with a contact electrification layer based on fluoropolymers [8,9] or silicones [10,11]. Many studies have employed indium-tin oxide (ITO) as transparent electrodes, but silver wires [12,13] and PEDOT (polyethylenedioxythiophene) [14] have also been used. It has also been shown that non-transparent edge electrodes allow integration with standard photovoltaic cells [15].

The first devices for water droplet energy harvesting using contact electrification were based on electrodes covered by a thin fluoropolymer film, where the drop was contacted by [16] or dripped [17] onto the device. Various different such back-electrode designs have been reviewed [18,19]. Devices and structures for harvesting electrical energy from the kinetic energy of water droplets are depending heavily on the development of materials for optimal solid-water contact electrification. Devices utilizing periodically contacting water droplets [20], sloshing water waves [21] or sliding droplets [22,23] have received considerable attention. Various multifunctional wearable materials for this purpose are considered [24,25], but also devices based on commercially available fluoropolymers have been studied [26,27]. The physical mechanisms of droplet impact [28] reveal that they play a major role for the amount of energy that can be harvested [29]. A range of different devices have been created based on contact electrification between solids and liquids, thus opening up new ways to power small sensors. These devices are based on monitoring the charge generated during pipetting [30], dripping [31] or transition through an interface [32]. Sensors for monitoring liquid level [33], microfluidic flow [34,35], self-powered distress signal emitters [36] and devices for optical communications [37,38] have been developed. Air bubbles in water [39] and fluid-elements [40,41] have been utilized in energy harvesting based on contact electrification with the aim of monitoring ion concentration [42], liquid leakages [43], turbidity [44] and pH [45]. The design of self-powered sensors relies on the design of coatings [46] and electrodes [47], where the surface roughness is of crucial importance [48,49]. New sensors for gas-detection rely on contact electrification [50,51]. Encapsulation of liquids in containers [52,53] or novel materials [54–56] may open up new applications in self-powered sensing. However, the performance is ultimately determined by the design of electrodes [57–59], contacting surfaces [60–62] or contacting scheme [63,64]. Inspiration for the design of surfaces is found in nature, where both man-made [65] and natural [66] surfaces are considered for contact electrification. In addition to the surface structure [49,67,68], also the amount of charge put into the surfaces by external means control how much charge can be harvested [69,70]. Moreover, also surface liquid infusion may influence the electrical output performance [71–73]. The charge transfer is mainly governed by the charge available [74–76], and precharging of polymer films as well as careful front-electrode designs which allow feedback have paved the way for improved devices [74,77,78].

Recent studies have demonstrated that front-electrodes can be used to improve the water-drop energy harvest [27,44,59,74,75]. However, there is a need to understand how to balance the performances of the photovoltaic and water-drop energy harvester to the particular application. In the current study the water-drop energy harvester utilizes a front-electrode that is either transparent or hidden, in the sense that it does not block light, is utilized in a device for both harvesting energy from water droplets as well as light. Three different contact electrification devices utilizing hidden or transparent front electrodes are investigated, with particular emphasis on integrating its functions in presence of a photovoltaic solar cell. To do so, issues related to transmission of light as well as mechanical to electrical energy conversion are studied with the goal of finding a design which allows utilization of existing materials.

2. Water drop energy harvesting using flat hydrophobic film and edge electrodes

The first device presented in this work is shown in Fig. 1 a), and is a minimal version wherein the contact electrification layer is placed directly on top of the photovoltaic cell and fastened with adhesive. The metal electrode is then wrapped around the rim of the photovoltaic cell. If one has the materials available (photovoltaic cell, contact electrification layer and metal electrode), the whole fabrication process is very simple only takes a few minutes. Fig. 1 a) shows a picture of a commercial polycrystalline solar cell with a hydrophobic contact electrification layer on top, and electrodes placed at the edges such that they do not block any illumination.

Fluorinated ethylene propylene (FEP) is a much-used hydrophobic fluoroplastic known for its ability to become triboelectrically charged and is therefore choses as contact electrification layer. Here a 50 μm thick film of FEP (DuPont) is used as contact electrification layer, which when impacted by water droplets develop a negative surface charge. The metal electrode is a 0.25 mm stripped nickel-coated copper wire wrapped around the edge of the photovoltaic cell such that it does not block the light. The metal electrode is used to collect charge, while at the same time remaining in the path of the water droplet to be able to collect the associated transferred charge.

The basic working principle is shown in Fig. 1 b)–d). The electrified film will cause the positive charge inside the droplet to move towards the water-solid interface upon impact. This charge is transferred when the droplet comes in contact with the metal electrode, and a current will run into the storage reservoir on the top electrode not in contact with water.

2.1. Electrical characterization

Upon letting water droplets of volume 60 μL impinging on the device from 0.3 m height, the current occurs as pulses with a positive and a negative return as seen in Fig. 2 a). This observation is in qualitative agreement with the mechanism outlined in Fig. 1 b)–d).

To be able to harvest energy from the device, it was connected to a resistive load, and the corresponding peak current versus load resistance R_L is shown in Fig. 2 b). The peak power of each water-droplet-induced pulse is shown as function of load resistance in Fig. 2 c). It is found that a peak power of about 40 μW is obtained when $R_L = 33$ MΩ. However, peak power is only reached for a few milliseconds, and perhaps the average power per water-droplet-induced electrical pulse would be a better measure. To this end, the blue circles in Fig. 1 c) suggests that the average power per pulse is about 4 μW at $R_L = 33$ MΩ. By integrating the power $R_L \int I^2 dt$ over one single pulse due to a single water droplet it is found that about 0.12 μJ is harvested.

2.2. Transmittance of light and photovoltaic solar cell performance

The performance of a photovoltaic solar cell depends strongly on how much light passes through the hydrophobic film in front of it. In many cases, glass or plastic covers are used to protect the solar cell, which means that the application of a contact electrification layer would not hamper the performance of the solar cell if both the contact electrification layer and the underlying electrodes are entirely transparent to sunlight. However, complete transparency is seldom the case, and it is

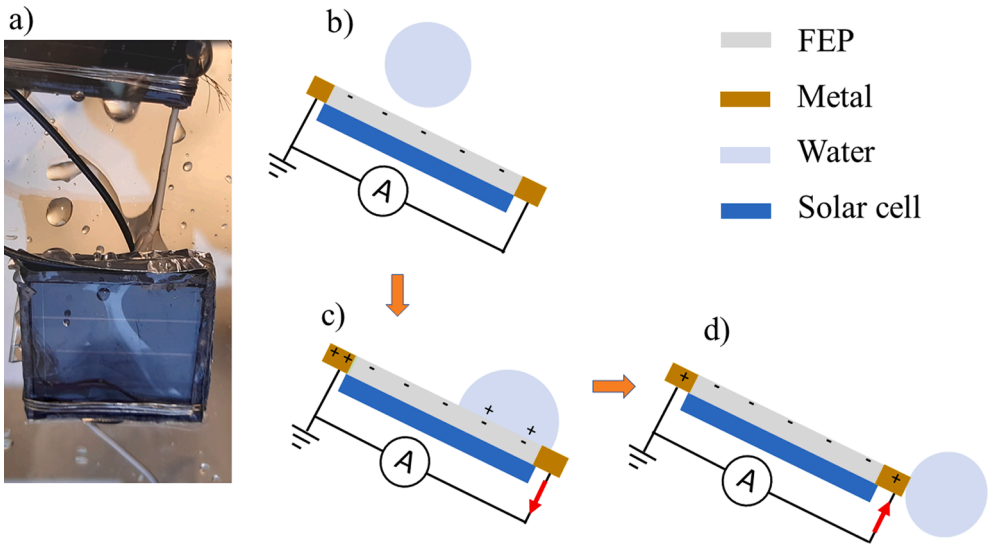

Fig. 1. A picture of a device utilizing non-transparent metal electrodes (a), and schematic drawings of its working principle (b-d). See the text for details.

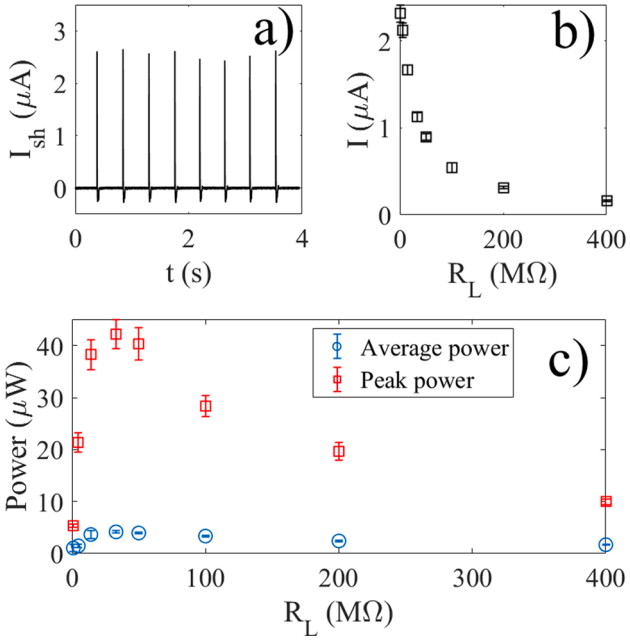

Fig. 2. The short circuit current (a) when individual water droplets of volume 60 μL impinge on the device from a height of 0.3 m. In b), the peak current is displayed as a function of load resistance of an external resistor. In c), the peak power (red squares) and average power (blue circles) of each pulse is shown as a function of load resistance. (For interpretation of the references to colour in this figure legend, the reader is referred to the web version of this article.)

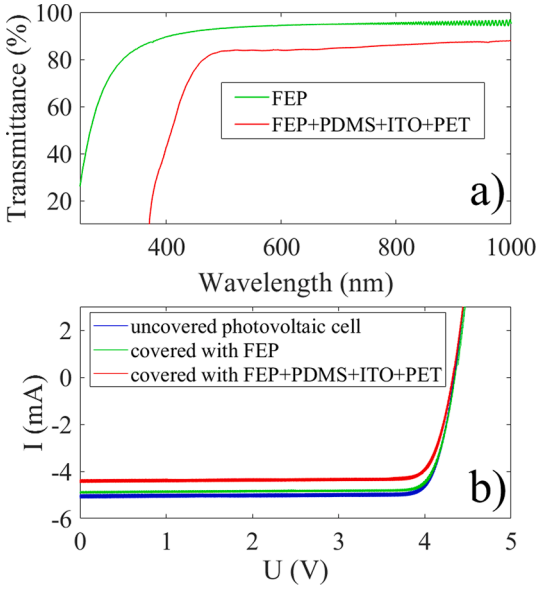

Fig. 3. In a), the transmittance with FEP (green line) and FEP + PDMS + ITO + PET (red line) is shown. In b), the current versus voltage of a solar cell is shown for an uncovered solar cell (blue line), solar cell covered with FEP (green line) and a solar cell covered with FEP + PDMS + ITO + PET (red line). (For interpretation of the references to colour in this figure legend, the reader is referred to the web version of this article.)

therefore necessary to evaluate the transmittance of these components before mounting them on a solar cell.

The green line in Fig. 3 a) shows the transmittance of the 50 μm thick film of FEP film measured using an UV-VIS spectrometer. In most of the relevant spectrum the transmittance remains above 95%, but in the ultraviolet region (<400 nm) it drops to below 90%. However, in many solar cells this has no consequence due to their low UV-performance.

In Fig. 3 b), the current versus voltage of a solar cell is shown for an uncovered photovoltaic cell (blue line) of efficiency $\eta = 0.044$ that is illuminated by collimated halogen lamp light of 450 W/m^2. The green line in Fig. 3 b) shows the current versus voltage for the same photovoltaic cell under the same illumination conditions, but now covered with a 50 μm thick FEP film. Upon covering the solar cell with FEP, the short circuit current drops from 5.0 mA to 4.8 mA, corresponding to a ratio 4.8/5.0 = 0.96, in good agreement with the transmittance observed in Fig. 3 a). The corresponding drop in electrical power is about 0.2 mA•4V = 800 μW, which is about 20 times higher than the peak power produced using from harvesting electrical energy using water droplets.

3. Water drop energy harvesting using flat hydrophobic film and a transparent electrode

Another device configuration that allows utilization of electrostatic induction more efficiently than the design in the previous section is when a transparent electrode is placed below the contact electrification

layer. The transparent electrode should have maximum transmittance in the part of the light spectrum where the photovoltaic cell operates. Fig. 4 a) shows a picture of a commercial polycrystalline solar cell with a water drop energy harvesting cell tightly attached using a 0.1 mm thick layer of Polydimethylsiloxane (PDMS) as waterproof and transparent adhesive. Here ITO is used as back electrode and front electrode in order to have an all-transparent electrode system. In the lower picture in Fig. 4 a) the rain cell is held at an angle such that the structure of the ITO electrode can be seen more clearly. This structure is drawn schematically from the side in Fig. 4 b).

When the droplet comes in contact with the contact electrification layer (FEP) and then subsequently with the front-electrode made by ITO, the formation of a water-solid electrical double layer causes the electrons to move into the back-electrode made by ITO to neutralize the positive charge, such that an electrical current flows as shown in Fig. 4 c). When the water droplet retracts from or moves away from the contact electrification layer, the water-solid electrical double layer mostly disappear (unless small amounts of water remain on the surface) and the electrons move out of the protected ITO electrode to generate a current as shown in Fig. 4 d).

3.1. Electrical characterisation

Upon letting water droplets of volume 60 μL impinging on the device from 0.3 m at a volume rate $R_V = 0.1$ mL/s, the open circuit voltage of the rain cell is about 30 V as shown in Fig. 5 a), whereas the short circuit current peak is about 5 μA as seen in Fig. 5 b). The electrical power generated is conveniently classified either through the peak or average pulse power in each pulse as a function of external resistive load R_L. Fig. 5 d) shows the peak power (red squares) and average power (blue circles) of each current peak as a function of resistive load. At $R_L = 33$ MΩ, the peak power is maximum of about 250 μW, whereas the average power in each pulse is about 40 μW.

The amount of electrical energy deposited in the resistive load can be found by integrating the power $R_L \int I^2 dt$ over one single pulse due to a single water droplet. The electrical energy harvestable at the optimum load is about 1 μJ. On the other hand, the potential energy of the 60 μL drops falling from a height of 0.3 m is mg ≈ 176 μJ, which means that about 0.6% of the mechanical potential energy is transformed into electrical energy. It is likely that the actual conversion efficiency is higher, since not all the mechanical potential energy is transformed into kinetic energy in the water droplets. It is also seen that while 0.6% is the largest efficiency of the devices compared in the current work, it is still smaller than some previous studies where precharging has been used [74,75]. However, it should be emphasized that in the current work none of the devices have received any particular pretreatment except simple rinsing and cleaning in deionized water, and all the devices have been assembled directly from prefabricated, commercially available parts.

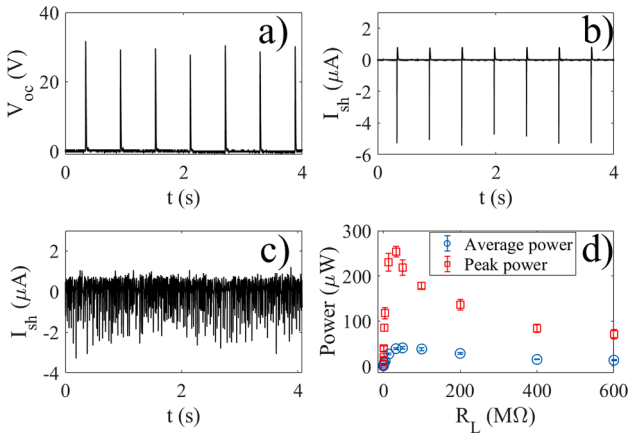

Fig. 5. The open circuit voltage (a) and the short circuit current (b) when individual water droplets of volume 60 μL impinge on the rain cell from a height of 0.3 m. In c), the short circuit current due to water volume rate of 2.5 mL/s is shown. In d), the peak power (red squares) and average power (blue circles) of each current pulse are shown as function of load resistance. The device is tilted at an angle of about 30°. (For interpretation of the references to colour in this figure legend, the reader is referred to the web version of this article.)

3.2. Current fluctuations versus volume rate

Studies have shown that increasing the volume rate from very small to large does alter the current characteristics in a complex manner [15,26]. An example of the short circuit current under higher flow rates is shown in Fig. 5 c), where the same nozzle that outputted 60 μL water droplets in Fig. 5 b) is opened entirely to allow the outlet of a laminar stream of volume rate $R_V = 2.5$ mL/s from a height of 0.3 m. While the stream is laminar right after the nozzle, instabilities cause breakup into droplets right before the surface, and it is observed that there is great variability in current and charge associated with each pulse.

Fig. 6 a) shows the average of short-circuit current peaks as a function of volume flow rate. At low volume rates individual droplets are observed from the nozzle, each impinging on the FEP surface below.

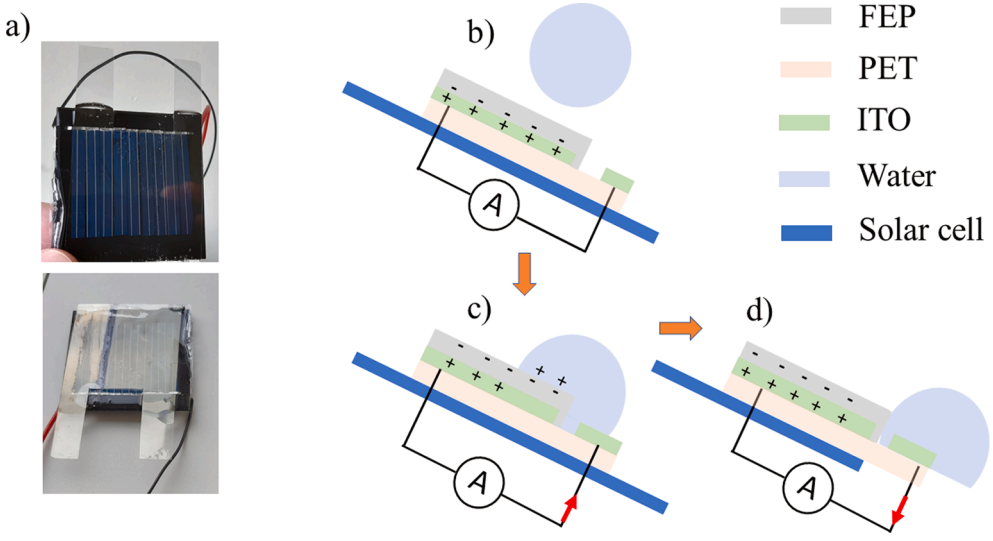

Fig. 4. A picture of a device utilizing transparent ITO-electrodes (a), and schematic drawings of its working principle (b-d). See the text for details.

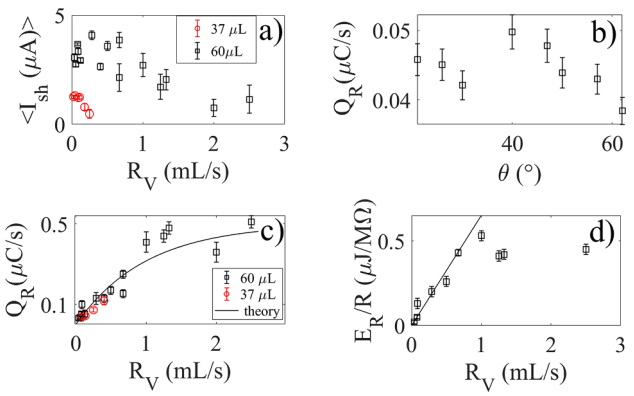

Fig. 6. In a), the average of short-circuit current peaks is shown when individual water droplets of volume 60 μL (black squares) and 37 μL droplets (red circles) impinge on the rain cell from a height of 0.3 m. In b), charge transfer rate is displayed versus tilting angle for a volume rate of 0.1 mL/s, whereas in c) the charge transfer rate is given as a function of volume flow rate for 37 μL droplets (red circles) and 60 μL droplets (black squares). The solid line in c) is a fit of Eq. (1) to the experimental data. In d), the harvestable energy E_R/R is plotted as a function of volume rate, where the solid line is a linear fit to the data at small volume rates. (For interpretation of the references to colour in this figure legend, the reader is referred to the web version of this article.)

Under such conditions, each current pulse is clear and separated as in Fig. 5 b). Above 0.7 mL/s, the flow out of the nozzle becomes laminar, and an unstable streak occurs after falling a few cm, thus causing a fluctuating stream that breaks up into droplets at the FEP surface. It is also observed that the current peaks start to vary more significantly. These fluctuations are expressed through the decrease in average peak current as well as an increase in the uncertainty (error bars) in Fig. 6 a). It is noted that the nozzle diameter plays a role here, as with thinner nozzles giving smaller droplets there is an earlier onset of laminar streaming followed by fluctuating breakup near the surface. However, these details depend much on the particular setup used, and are therefore outside the scope of the current work.

3.3. Influence of tilting angle

The static contact angle of a pristine FEP surface is about 110° [49], and the surface must be tilted for droplets to move away. The output power of photovoltaic cells is known to depend on the incident angle of the light, and one needs to investigate whether the tilting angle of the device with respect to the falling water does play any role also for water drop energy harvesting. In the current work, the peak short-circuit current did exhibit something that appears to be a peak in the angular range between 40 and 50 , but the fluctuations were too large to allow one to draw a clear conclusion. Also, the charge transfer demonstrated a similar tendency, as depicted in Fig. 6 b). Here, the total charge transfer per second (Q_R) at 0.1 mL/s is found by integrating the current over a time interval containing many pulses and then divided by the number of pulses. It is seen that the total charge transfer rate does not exhibit a very clear peak with angle, thus confirming the trend observed for the peak currents. It should be pointed out that angle-dependency of the current or charge transfer rate depends on factors such as the thickness and roughness of the front-electrode as well as the wetting properties of the hydrophobic film as well the front-electrode, thus making it strongly device geometry and surface-dependent.

Despite a rather weak angle-dependency found in this study, it is clear that the surface must be tilted for the water droplets to be removed. Research has shown that for droplets of volume 5 μL, the critical tilting angle to start movement down an untreated FEP surface can be as large as 70° [15]. For 60 μL droplets this critical angle decreases to below 20°. For a superhydrophobic, nanostructured FEP surface, the critical angle above which small droplets start to move is much smaller, but still above 10° for small 5 μL droplets. Thus, it might seem advantageous to use a superhydrophobic surface. However, care should be taken, since roughness-induced increase of the contact angle may decrease the contact charge transfer [49], which therefore also reduces the voltage. Fig. 7 a) shows a finite element simulation of the water drop energy harvesting device under open circuit potential ($R_L \to \infty$) performed in COMSOL 5.4 for a 3 mm diameter drop with a contact angle of about 110 with the FEP film (blue) moving towards the front-electrode held at zero potential (red brown). The red circles in Fig. 7 b) show the corresponding open circuit potential V_{oc} between the front-electrode and a floating electrode placed under the FEP film. As in Fig. 5 a), V_{oc} is set to zero in absence of a droplet. Note also that $\Delta z = 0$ mm is defined as the position where the water first comes in contact with the lower metal electrode. As the static contact angle increases, the voltage decreases due to less electrostatic coupling between water and FEP. The smallest coupling is expected to occur for a static contact angle of 180 . For comparison, also the open circuit potential in the case of a water droplet forming a contact angle of 180 is shown as black squares in Fig. 3 b). It is seen that the maximum voltage difference in the superhydrophic case is about 9 V and occurs when the water droplet is directly above the transition from dielectric and conductor. In the case of 110 contact angle, the maximum voltage difference is about 14 V and last while the droplet is contact with both dielectric and electrode. This is qualitatively consistent with the observed behavior of the voltages in Fig. 5 a).

The simulations of Fig. 7 suggests that there is no advantage for electrical energy harvesting using a superhydrophobic FEP film. In fact, smaller contact area with the hydrophobic film reduces the electrostatic coupling. This is in line with the findings of Ref. [49], where it was demonstrated that the charge transfer is smaller for superhydrophobic surfaces. However, it is also known that creating superhydrophic surfaces using for example electron beams, could implant charge which could improve the electrical performance. However, such effects should be considered separately, and not be confused with superhydrophobicity alone. In the current work the goal was to create hybrid devices assembled from easily commercially available materials without the need for complicated materials processing. Since one cannot create superhydrophobic surfaces from FEP in a simple manner maintaining or improving the surface charge density in a reliable manner, pristine FEP surfaces were chosen.

3.4. Charge transfer versus volume rate

In Fig. 6 c), the total charge transfer per second (Q_R) is measured as a function of volume rate for a fixed tilting angle of 30 for nozzles allowing either 60 μL (black boxes) or 37 μL (red circles) water droplets. It is seen that the charge transfer rate at first increases with volume rate. The smaller nozzle could not output volume rates beyond 0.4 mL/s, but

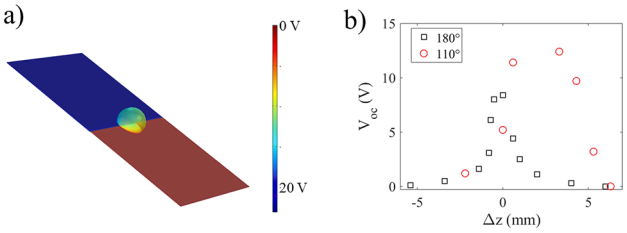

Fig. 7. Finite element simulations of a water droplet sliding down the incline while the contact angle remains static at 110 (a). In b), the open circuit potential is shown as a function of displacement of the water droplet for contact angles 110 (red circles) and 180 (black squares). The colors represent the electrical potential at open circuit conditions, with the front-electrode grounded and the back-electrode at floating potential. The droplet has radius 3 mm and the surface charge density is -0.1 μC/m^2. (For interpretation of the references to colour in this figure legend, the reader is referred to the web version of this article.)

it is nonetheless seen that the charge transfer rate follows the same trend for small and large droplets. Above 1 mL/s, the charge transfer rate appears to saturate.

The saturation can be modelled using simple arguments. Initially the charge transfer rate is determined entirely by individual droplet passing over the front-electrode one-by-one without interaction. As the number of droplets increase, they start to interact by forming a more or less continuous stream and therefore partially block the charge transfer that occurs along the direction of spreading upon impact. On the other hand, transversal fluctuations perpendicular to the motion down the FEP surface increase with volume rate up to a certain threshold. Assume that the number of droplets N that can contribute to charge transfer per volume is governed by a simple continuous rate equation, $dN/dV=(N_0-N)/V_0$, where N_0 is the maximum number of droplets before a continuous stream occurs down the slope and V_0 is the maximum volume of the droplet stream in an instant of time. Furthermore, we note that each droplet can be associated with an average charge transfer q, such that the total charge transfer rate is $Q_R = d(Nq)/dt$. The maximum charge transfer rate is then $Q_{R0} = d(N_0q)/dt$. It should be noted that $dQ_R/dR_V = [d(qN)/dt]/[dV/dt] = qdN/dV$ and $(N_0-N)/V_0 = (Q_{R0} - Q_R)/R_{V0}$, where R_{V0} is the maximum volume rate before a continuous stream occurs. One can then write the differential equation as proportional to difference between the maximum number of droplets the $dQ_R/dR_V=(Q_{R0}-Q_R)/R_{V0}$, which can be solved with the initial condition $Q_R(Q_R = 0) = Q_{R0}$ to give

$$Q_R = Q_{R0}\left(1 - e^{-\frac{R_V}{R_{V0}}}\right) \quad (1)$$

The solid, black line in Fig. 6 c) shows a fit of Eq. (1) to the experimental data with $R_{V0} = 1$ mL/s and $Q_{R0} = 0.5$ μC. While this model is rather simple, it does capture the essential observation that interactions between droplets does play a role for charge transfer, as was also observed in the case of devices utilizing back-electrodes only [26].

3.5. Does the droplet-generated energy scale with water volume rate?

Falling water drops have a certain kinetic energy given by the volume rate, which is converted into electrical energy using the devices described in the current work. An interesting question is whether the harvestable electric energy increases in the same manner as the kinetic energy with increasing volume rate.

The water drop intensity R_{SI} is measured in meters per seconds or millimeters per hour, and is defined as the volume of water filled up in a tank per area and time. If we imagine that a tank of cross-sectional area A is filled from empty to a water level Δz in the time interval Δt, the average water drop intensity is given by $R_{SI} = \Delta z/\Delta t$. The water drop intensity is related to the volume rate by $R_V = AR_{SI}$, where the water volume $\Delta V = A\Delta z$ is generated by N droplets of the same volume V_i. It is seen that $R_{SI} = \Delta z/\Delta t = A\Delta z/A\Delta t = NV_i/A\Delta t$, and the water volume can also be expressed as $\Delta V = NV_i = R_{SI}A\Delta t$. The kinetic energy of one water drop is given by $E_{k,i}=(1/2)\rho V_i v_T^2$, where ρ is the density of water, $m_i = \rho V_i$ is the mass and v_T the velocity of the water drop. The total kinetic energy of the N noninteracting water droplets is therefore given by $E_{k,tot} = NE_{k,i} = (1/2)\ \rho\ NV_i v_T^2$. Upon using $NV_i = R_{SI}A\Delta t$, the total kinetic energy of the droplets impinging per area can be expressed as

$$E_{k,tot} = \frac{1}{2}\rho v_T^2 R_V \Delta t \quad (2)$$

or in terms of the water droplet intensity $E_{k,tot}/A=(1/2)\ \rho\ v_T^2 R_{SI}\Delta t$. Eq. (2) is a measure of the kinetic energy associated with the water drops, and it is clearly seen that it increases linearly with the volume rate.

Not accounting for droplet interactions, one might naively imagine that also the harvestable electric energy should increase linearly with volume rate. The amount of energy that can be harvested using a resistive load can be found as described above by integrating the power $R_L \int I^2 dt$ over a specific time interval. However, it appears that the optimum load changes slightly with volume rate since the impedance of the device depends on how much water is present. Here, it is of more interest to find out whether the harvestable energy follows a linear trend as suggested by Eq. (2), but now for an imagined small electrical resistance R. To this end, it suffices to evaluate the integral $E_R/R = \int I_{sh}^2 dt$, which is shown in Fig. 6 d) as a function of volume rate R_V. It should be pointed out that E_R/R provides a measure of the energy deposited at small resistive loads much smaller than the optimum load, not depending much on the device impedance or water-coverage. From Fig. 6 d) it is seen that E_R/R increases nearly linearly for small volume rates, as indicated by the fitted solid line. However, at volume rates exceeding 1 mL/s there is a tendency of saturation, as was also observed for charge transfer in Fig. 6 c). but tend to saturate above 1 mL/s. The fact that the harvestable energy no longer increases linearly with volume rate can be related to the onset of a more densely packed erratic droplet stream where the droplet interactions prevent the energy to be summed up as it would with independent droplets.

3.6. Transmittance of light and photovoltaic solar cell performance

The transmittance plays a crucial role for the performance of the photovoltaic cell, and is evaluated as a function of wavelength for a 50 μm FEP film glued with a thin layer of PDMS to ITO attached on PET in Fig. 3 a). It is found that the transmittance is between 85% and 90% for long wavelengths, but drops below 85% for wavelengths shorter than 500 nm. These measurements are done for normal incident light in a UV-VIS spectrometer, and in most cases, one also need to check the solar cell current-voltage performance with the materials mounted. The red line of Fig. 3 b) shows the current-voltage characteristics of the photovoltaic cell covered by FEP + PDMS + ITO + PET. Now the short circuit current has dropped to 4.3 mA, and the ratio 4.3/5.0 = 0.86 is again in reasonable agreement with the transmittance measurements. The corresponding drop in electrical power is about 0.7 mA•4V = 2400 μW, which is about 10 times higher than the peak power produced using from harvesting electrical energy using water droplets. Thus, the relative power loss is smaller than in the case of the device described in Section 3.

A layer of water or water droplets on top of the FEP film influences the performance of the photovoltaic cell through changes in the light transmittance. Water has a refractive index of about 1.33, which means that about 2% of the light is reflected from the air-water interface. Moreover, water has an absorption coefficient of the order of 0.1 m^{-1} [79]. The thickest water layer or biggest sized water droplets would be of the order of 1 cm, which means that about $100\exp(-0.1\ m^{-1} \cdot 0.01\ m) = 99.9\%$ of the light will be transmitted through the water without being absorbed. Moreover, since FEP has a refractive index very similar to water (about 1.34) [15], very little light is reflected at the water-FEP interface. The size distribution of water droplets that is incident on the contact electrification layer might play a role for both the water-drop energy harvested as well as the performance of the photovoltaic cell. Small droplets at reasonably low volume rates have a tendency of sticking to the surface, while larger droplets collide, deform and eventually roll off the surface. It is found that 5 μL water droplets placed on an FEP surface will remain stationary for tilting angles as large as 70° [15]. Larger 60 μL droplets only remain stationary for a tilting angle up to 20°. However, also smaller droplets fixed to the surface may grow as the influx of water continues, eventually becoming big enough to be teared apart by gravity and therefore start to move down the incline.

An attempt to measure the size distribution of water on a 50 μm thick FEP film after spraying it with water droplets is shown in Fig. 8 a).

In Fig. 8 b), the size of the droplets on the surface in Fig. 8 a) have been measured (752 droplets) and presented as a histogram (blue bars). It was checked by upon repeating the spray-on process with the same nebulizer and distance to surface the size distribution remained about

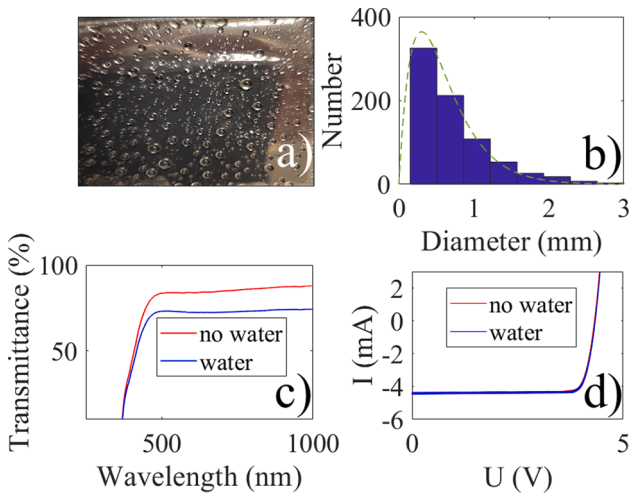

Fig. 8. Small droplets are sprayed on a FEP surface (a), and the size distribution is measured (b). The dashed green line is a fit of Eq. (3) to the experimental data. In c), the transmittance of a device covered with FEP + PDMS + ITO + PET is shown in absence (red line) and presence (blue line) of water droplets. In d), the current versus voltage curve for a solar cell fronted by the FEP + PDMS + ITO + PET rain cell and illuminated by 450 W/m^2 is shown in absence (red line) and presence (blue line) of water droplets. (For interpretation of the references to colour in this figure legend, the reader is referred to the web version of this article.)

the same. In Fig. 8 b), it is noted that the smallest droplets with sizes of about 0.3–0.5 mm are most abundant, i.e. droplets of volume < 0.1 μL. The size distribution can be well fitted with the formula that was first used to fit the size distribution of rain droplets from stratiform precipitation [80,81]

$$N(D) = N_0 D^{\varphi} exp(-\lambda D) \quad (3)$$

The dashed green line shows that the distribution in Eq. (3) provides a reasonable fit to the data with $\phi = 1$, $N_0 = 3300$ and $\lambda = 3.3$ mm^{-1}.

In Fig. 8 c), it is seen that the transmittance in measured by the spectrometer drops from about 85% at wavelengths above 500 nm (red line) in absence of water droplets to about 75% (blue line) in presence of water droplets when a device comprised of FEP + PDMS + ITO + PET corresponding to the red line in Fig. 3 a) is used. This drop in transmittance can be explained by the fact that curved surfaces of the droplets refract the almost parallel beam of light passing through the spectrometer, thus causing the spectrometer apertures to block parts of the light. In Fig. 8 d) the current versus voltage curve for a solar cell fronted by the FEP + PDMS + ITO + PET rain cell and illuminated by 450 W/m^2 halogen light is shown in absence (red line) and presence (blue line) of water droplets. It is seen that there is no observable change in the voltage-current characteristics by the presence of water droplets. This may seem puzzling, as the transmittance in the spectrometer did indeed show a significant change. However, it is explained by noting that the rain cell is in close contact with the photovoltaic cell, which means that most of the refracted and some of the reflected light from the water droplets illuminates the cell. In sum, the change in illumination by the presence of water droplets is very small when the FEP film is in close contact with the photovoltaic cell.

It should be pointed out that the small droplets in Fig. 8 a) are stuck at the surface, as it is difficult to obtain useful results for larger droplets that do not stick using the methods available here. The small droplets in Fig. 8 a) are not expected to produce significant current pulses even if they had been able to move down the incline towards the front-electrode. However, as the number of droplets build up with time, they eventually become big enough to detach, and such larger droplets may contribute to the electrical production, although not in the same manner as the directly impacting droplets studied in Fig. 5. Instead, there will be a combination of rolling and sliding as studied in Refs. [26,44,57]. Fig. 8 represents one possible situation where the entire surface is covered by droplets of volume typically smaller than 15 μL. In most realistic situations the water coverage will be smaller. For example, larger droplets moving off the FEP surface might only briefly influence the light transmittance. Since the current-voltage characteristics as well as the transmittance spectrum require some time to be acquired, the data are always the result of averaging. However, it is probably most useful to evaluate such averaging data under the specific water droplet source considered.

4. Water drop energy harvesting using curved hydrophobic film

The energy harvesting device presented in Fig. 4 has flat electrodes, thus requiring that the surface is tilted to allow the water drops to move off. The fact that all realistic surfaces require a tilt to clear water may pose a problem when water droplet energy harvesting is used together with photovoltaic cells. That is, under some circumstances it is advantageous if the photovoltaic cell could point in the same direction as the water drop comes from. With a flat design as in Fig. 4, this would naturally lead to a pile-up of water on the hydrophobic film, thus reducing performance.

One possible solution is to use a curved hydrophobic film in connection with curved transparent electrodes, to allow the solar cell to face directly upwards while at the same time providing the required surface inclination for the droplets to move downwards. An example of a design is shown in Fig. 9 a), where the PDMS is formed into a 3 cm cylindrical lens on which the protected ITO electrode and FEP contact electrification film are attached. The exposed electrode is a nickel-coated copper wire that runs around the rim of the cell, see Fig. 9 b). The reason for not using an ITO front-electrode was to make the device more robust. Although the device in Fig. 4 could be used with deionized water for weeks without any sign of degradation, it was found that contaminated water (e.g. low pH) would wash away parts of the ITO electrode and thus reduced the performance. Such problems were not found to be an issue using a nickel-coated copper wire as in Fig. 1 a) and 9b), although here a disadvantage is that the wire must be placed away from the lit area of the solar cell to avoid reduction of photovoltaic energy.

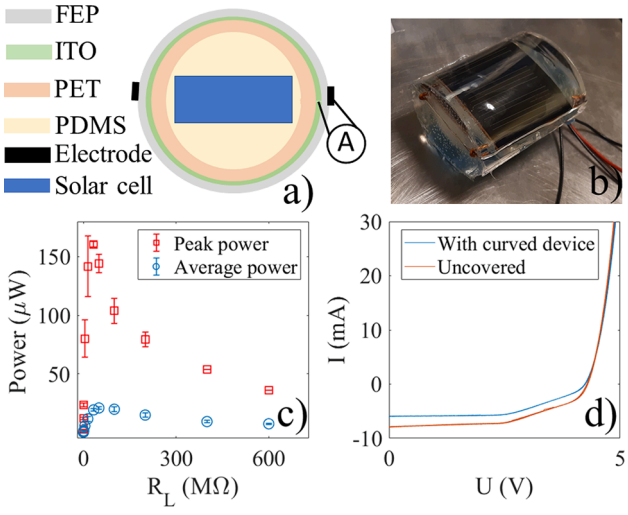

Fig. 9. Schematic drawing of a curved device (a), and a picture of the actual prototype (b). In c), the peak power (red squares) and average power (blue circles) of each current pulse are shown as function of load resistance. In d), the current versus voltage curve is shown for the bare photovoltaic cell before anything is attached (red line) as well as with the curved device as seen in b) (blue line). (For interpretation of the references to colour in this figure legend, the reader is referred to the web version of this article.)

Fig. 9 c) shows that the peak power is maximum of about 150 μW, whereas the average power in each pulse is about 20 μW, when 60 μL droplets are released directly on the top of the cylindrical rain cell from a height of 0.3 m. The harvestable energy and efficiency are therefore lower than for the flat device in Section 3. This could be related to the fact that the front-electrode had to be placed outside the lit area of the solar cell, where the water droplets splash of into smaller fragments before touching the wire or otherwise not properly contributing to charge transfer.

Another issue of concern is the electrical characteristics of the solar cell when covered by the cylindrical PDMS lens. While one may naively imagine that a cylindrical lens does collect more light onto the solar cell, it is important to remember that PDMS also does scatter and absorb light to some degree. In Fig. 8 d), the current versus voltage curve is shown for the bare solar cell before anything is attached (red line) as well as with the curved rain cell as seen in b) (blue line) upon illumination using collimated halogen light of 450 W/m^2. For unknown reasons, the commercial photovoltaic cell used here had a somewhat kinked current-voltage performance, but it was found to be stable and reliable for a further analysis. Before the solar cell is encapsulated in the rain cell, the short circuit current is about 8.0 mA, but drops to 6.0 mA after encapsulation. This corresponds to a ratio of 6.0/8.0 = 0.75, which shows upon comparison with Fig. 2 that the thick, cylindrical PDMS lens is scattering or absorbing some of the light. Clearly, the average power of 0.02 mW provided by the water drop energy harvesting device cannot compensate for the photovoltaic power loss which is two order of magnitude larger.

5. Discussion

The performance of the water-droplet energy harvesting of the curved device in Section 4 is better than the flat device in Section 2, but worse than that in Section 3. However, each of the devices have their own advantages and disadvantages. While the device in Section 3 gave the largest droplet-induced power, the photovoltaic energy loss is larger than that of the device in Section 2. The device in Section 4 had the largest photovoltaic loss, most likely due to scattering from the thick PDMS. Thus, a better optical material and a more elaborate curved design might improve the performance and even provide efficient focusing of light onto the photovoltaic cell. However, the device presented in Section 4 had an added advantage of avoiding pile-up of water if the device was not tilted, thus allowing more freedom when aligning the photovoltaic cell towards the light source.

It is important to realize that the power reported in Figs. 2, 5 and 9 is that available before passing the signal through the processing and storage electronics. While the losses associated therewith have not been a topic in the current work, it is worth mentioning some related issues. First of all, it is clear that the time-varying signal from the water-drop energy harvester requires rectification before energy storage while that of the photovoltaic cell does not. For this purpose, the same rectification and storage system as in Ref. [26] was employed. That is, the electrodes were connected to a bridge rectifier (DF005M, Fairchild Semiconductor) and a 33 μF capacitor. If both the electrodes of the photovoltaic cell and the water-drop energy harvester are simultaneously connected to the bridge, one observes that the signals are superimposed as seen in Fig. 10 a). For t < 2 s, no water is flowing, while for t > 2 s water droplets are hitting the FEP surface. It is seen that the current is superimposed and therefore fluctuating with droplet arrivals, which means that this is an inefficient method to harvest energy. Instead, the energy from the two devices must be processed differently before storage. The simplest approach that allows direct comparison of the energy stored in the two devices is to use a bridge rectifier and a capacitor to store the energy from the water drop energy harvester, and a separate capacitor directly for the photovoltaic cell.

To illustrate how energy is stored in a 33 μF capacitor connected to the electrodes of a photovoltaic cell, Fig. 10 b) shows the measured

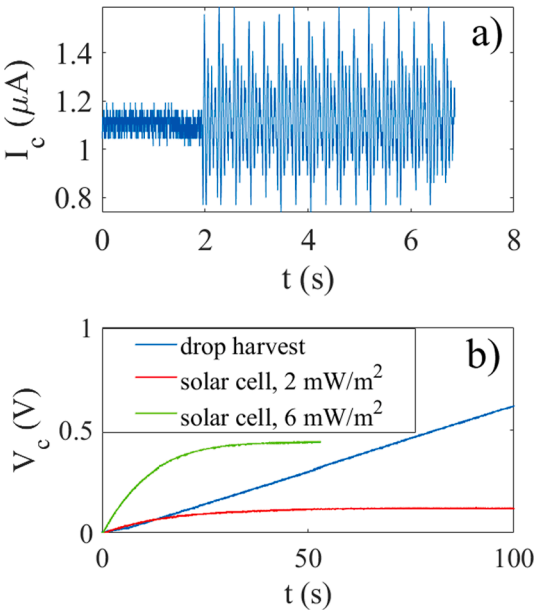

Fig. 10. In a) the current output from the bridge rectifier connected to a photovoltaic cell (when t < 2 s) and connected to both the photovoltaic cell and the water drop energy harvester (t > 2 s). In b) the voltage over a 33 μF capacitor is displayed as function of time when connected to a photovoltaic cell illuminated by sunlight of intensity 2 mW/m^2 (red line) or 6 mW/m^2 (green line). The blue line in b) shows the voltage over the 33 μF capacitor connected to a bridge rectifier attached to the water drop energy harvester in Fig. 4 exposed to water drops. (For interpretation of the references to colour in this figure legend, the reader is referred to the web version of this article.)

voltage as function of time for sunlight-illumination of 2 mW/m^2 (red line) and 6 mW/m^2 (green light). The sunlight intensity was controlled by putting the whole device in a box of variable opacity with a small opening to allow water droplets to hit the FEP surface from above in the same manner as in Fig. 5. For comparison, the blue line in Fig. 10 b) shows the voltage over the 33 μF capacitor connected to a bridge rectifier attached to the water drop energy harvester used in Fig. 5 when water drops are impacting the FEP surface through the hole in the opaque screen. In Fig. 5, each droplet generates an electrical pulse of average power about 40 μW. However, it should be noted that the pulses are short and far apart, such that the average power during the entire experiment is of the order of 0.5 μW for the optimal resistive load (R_L = 33 MΩ). In Fig. 10 b), the blue line indicates that capacitor collects electrical energy at a rate of the order of CVdV/dt ≈ 0.1 μW, which is much smaller than what one expects using an optimal resistive load (R_L = 33 MΩ). This due to the fact that the some of the energy is lost in the circuit (e.g. the bridge rectifier) and that that the capacitor used is not an ideal load. Even though a more efficient energy collecting electronics scheme can be used, there would still be losses associated with it not directly related to the performance of the water drop energy harvesting scheme. For this reason, it might seem more accurate to use the average power, either per pulse or per experimental interval, as a measure of the available power from the device. Thus, a consistent and correct manner to list the power of such hybrid devices is as demonstrated in Figs. 2, 5 and 9.

The total power delivered by the devices considered in this work is a sum of the contributions from the photovoltaic cell (P_{light}) and the water-drop energy harvester (P_{drop}). Since the power delivered by the latter comes in pulses due to water-drop impact, it is perhaps more convenient to compare the average power $< P_{drop} >$ associated with drop impact. On the other hand, if the light source is not fluctuating, the harvested power from light remains constant such that $P_{light} = <P_{light}>$. Note also that $< P_{light} > = \eta TIA$, where T is the transmittance of the water drop harvester placed on top of the photovoltaic cell, I is the

illumination intensity (in W/m^2), A is the area and η is the efficiency of the photovoltaic cell. A measure for the average power during a water drop impact is then P_{tot}=<P_{light}>+<P_{drop} >. From Fig. 10 b) it is seen that initially the energy deposition rate in the capacitor is similar for the water droplet energy harvester and the photovoltaic cell if the latter is illuminated by sunlight of intensity 2 mW/m^2. This is as expected, since the power generated by the photovoltaic cell at I = 2 mW/m^2 is < P_{light}>=ηTIA ≈ 0.1 μW for η = 0.044, T = 0.86 and A≈ 1.5•10^{-3} m^2 (the area of the photovoltaic cell in Fig. 4). It is also seen that the maximum energy stored in the capacitor is limited by the low voltage over the photovoltaic cell under weak illumination. The energy stored in a capacitor due to water drop energy harvesting can be much higher since the input voltage is much higher as seen in Fig. 5 a).

Fig. 11 shows an example of the total power as a function of illumination intensity for a photovoltaic cell with efficiency η = 0.044 (4.4%) assuming an upscaled system with A = 1 m^2. The blue line corresponds to < P_{drop}>=4 μW and T = 0.96. Here it is assumed that the average droplet-collected electrical power over the entire surface is the same as the maximum pulse-averaged power reported in Fig. 2. It is seen that when the illumination exceeds 0.1 mW/m^2, the output of the photovoltaic cell dominates the performance. For a water-drop energy harvester with < P_{drop}>=40 μW and T = 0.86 (black line), an illumination intensity exceeding 1 mW/m^2, is required for the photovoltaic cell. If the transmittance due to the transparent electrodes is reduced to T = 0.16, this illumination intensity increases by an order of magnitude. Also shown is a projected case with < P_{drop}>=400 μW and T = 0.96 (red-dashed line), which also requires an illumination intensity exceeding 10 mW/m^2 for the photovoltaic device to become dominating. Intensities in the range 0.1–10 mW/m^2 are very low and most likely to occur in absence of normal daylight or other strong light sources. Curves such as those displayed in Fig. 11 can help evaluate the performance under different circumstances, including outdoor use.

One possible application of the type of hybrid device considered in this work is in outdoors applications in sunlight and rain. If used in rain, the water droplet energy harvester considered here has been named a *rain cell* [29]. Here, the water droplets usually come down with a size distribution as well as a terminal velocity governed by size and wind, thus complicating the estimates of the harvestable energy. However, it is possible to make simple estimates. For example, the city of Bergen (the location of the author) had an annual rain level of 3101.7 mm in 2015, which corresponds to an average daily downpour of 0.35 mm/hour or

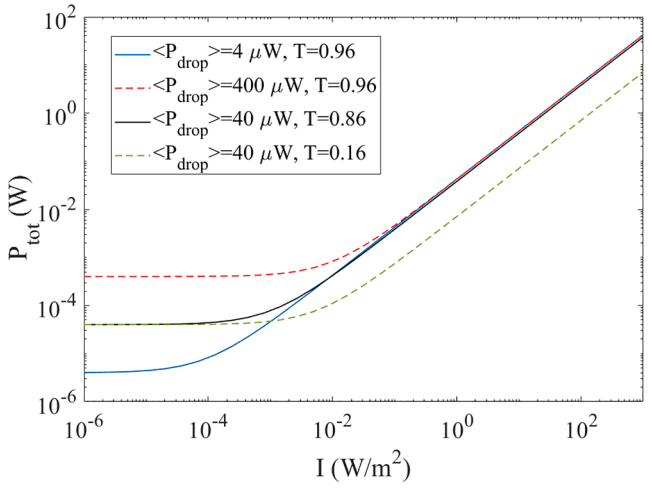

Fig. 11. The total power as function of light illumination intensity for a photovoltaic cell with η = 0.044 when < P_{drop}>=4 μW and T = 0.96 (blue line), <P_{drop}>=40 μW and T = 0.86 (black line), <P_{drop}>=40 μW and T = 0.16 (green dashed line), and < P_{drop}>=400 μW and T = 0.96 (red-dashed line). (For interpretation of the references to colour in this figure legend, the reader is referred to the web version of this article.)

R_{SI} = 9.72•10^{-8} m/s. Similar high rain intensities can be found in regions of Asia, Africa, and America. This rain intensity corresponds to the lower end of the volume rates reported in Fig. 6. The terminal velocity depends on the droplet size, which again depends on the rainfall intensity. It has been found that for droplets in stagnant air at normal pressure (1 bar) and temperature T = 20 °C the experimental data for the terminal velocity is well-fitted by the following equation [29]:

$$v_T = v_O\left[1 - e^{-\left(\frac{D}{D_0}\right)^n}\right] \tag{4}$$

where v_0 = 9.43 m/s, D_0 = 1.77 mm and n = 1.147. The maximum terminal velocity is typically reached when D > 3 mm, thus suggesting that larger droplets have a terminal velocity close to v_0. The droplet size distribution is not normally recorded in databases, but one can be certain that most droplets fulfil D < 3 mm, and a simple estimate may suggest v_T≈ 5.9 m/s if D ≈ 1.5 mm upon using Eq. (4). In addition, one has ρ = 1000 kg/m^3 and for a year Δt = 31 557 600 s, which inserted in Eq. (2) gives a kinetic energy per area of the order of 53 kJ/m^2 (or about 15 Wh/m^2). For a household requiring about 16 MWh of electrical energy per year, an area of 16 MWh/(0.006•15 Wh/m^2)≈ 1.8•10^8 m^2 is needed assuming that 0.6% of the kinetic energy of the rain is transformed into electrical energy. Clearly, large areas are needed to power such households. Even if one could increase the energy conversion to about 10% using the recent designs of Refs. [74,75], the area needed would remain very large and not practical feasible.

To this end, scalability is an issue that needs to be addressed if practical applications of rain cells are to be developed. Comparing different previous research on the type of front-electrode type water drop energy harvesters considered here (but without the photovoltaic cells), it appears that the electrification layer plus the front electrode must have an extension of size of the order of the droplet size or larger in order to generate the full charge transfer [44,47,76,78]. The droplets impact and spread on the surface, and eventually transfer the built-up charge into the front-electrode. If the available area is too restricted, there will not be sufficient charge transfer. The current study has used contact electrification areas large enough not to restrict droplet spreading dynamics or charge transfer during impact. It was found that photovoltaic cells with areas down to about 4 cm^2 would not reduce the performance of the water droplet energy harvesting system. Putting many cells together using the idea of a network presented in Ref. [47], this would allow one to create a large number of individual devices that could be put together to generate a larger amount of energy if the areas are available.

The output electrical power from the water droplet energy harvesting system investigated in the current work has relied on pure water. The author as well as other researchers have demonstrated that the ion concentration [20,27] as well as pH [44] may impact the amount of electrical energy that can be harvested. Very small amounts of ions as found in dirty rain might sometimes enhance the charge transfer, but it might also reduce it depending on the concentration. It is known that rain take on a typical pH values between 5 and 7, depending on whether acidic or alkaline components are present [82,83]. As demonstrated in Ref. [44], reducing the pH below 7 would reduce the electrical charge transfer slightly for front-electrode systems as considered in this paper. However, the reduction is only severe if the pH drops below 5, which is unlikely in most scenarios of interest.

If mounted outdoors, the combined photovoltaic and water droplet energy harvesting device provides high output energy during day with the major contribution from the photovoltaic device. At night, in absence of sunshine small electronic devices, e.g. turbidity sensors, CO_2 or pH sensors [44,45], can be powered if there is sufficient amount of water downpour. Thus, such combined energy harvesting devices might have applications in environmental sensors put in remote locations where sunlight is lacking in large parts of the day, and where batteries

are an unwanted option for storage and backup.

6. Conclusion

The aim of this work has been to investigate a combined photovoltaic and water droplet energy harvesting device where the latter utilizes a transparent or hidden front-electrode. Several new findings are reported in this article. It is demonstrated that a water drop energy harvester with an edge-electrode reduces the solar cell output energy less than a back-electrode. It is also demonstrated that the edge electrode provides smaller output power per water drop than the back-electrode. These issues must be considered when designing water energy harvesters to be mounted on photovoltaic cells.

Different arrangements and geometries were investigated in order to optimize the influx of light to the photovoltaic cell also in presence of water drops. It was demonstrated that the water drop-induced charge transfer fluctuates in a volume-rate dependent manner, thus leading to saturation also in harvestable energy at higher volume rates. The device reported may have outdoor applications, although considerable work on large-scale improvements of the mechanical-to-electrical energy efficiency as well as scalability is needed before this can take place.

Declaration of Competing Interest

The authors declare that they have no known competing financial interests or personal relationships that could have appeared to influence the work reported in this paper.

References

[1] Guigon R, Chaillout JJ, Jager T, Despesse G. Harvesting raindrop energy: experimental study. Smart Mater Struct 2008;17:015039. https://doi.org/10.1088/0964-1726/17/01/015039.

[2] Ahmad MA. Piezoelectric water drop energy harvesting. J Electron Mater 2014;43:452–8. https://doi.org/10.1007/s11664-013-2826-2.

[3] Ilyas MA, Swingler J. Piezoelectric energy harvesting from raindrop impact. Energy 2015;90:796. https://doi.org/10.1016/j.energy.2015.07.114.

[4] Wong CH, Dahari Z, Manaf AA, Miskan MA. Harvesting raindrop energy with piezoelectrics: a review. J Electron Mater 2015;44:13–21. https://doi.org/10.1007/s11664-014-3443-4.

[5] Viola F, Romano P, Miceli R. On the harvest of rainfall energy by means of piezoelectric transducer. In: International Conference on Renewable Energy Research and Applications (ICRERA); 2013. p. 1133–8. https://doi.org/10.1109/ICRERA.2013.6749923.

[6] Wong CH, Dahari Z, Manaf AA, Miskan MA. Piezoelectric beam length optimization for raindrop energy harvesting application. Appl Mech Mater 2015;705:247–51. https://doi.org/10.4028/www.scientific.net/AMM.705.247.

[7] Gart S, Mates JE, Megaridis CM, Jung S. Droplet impacting a cantilever: A leaf-raindrop system. Phys Rev Appl 2015;3:044019. https://doi.org/10.1103/PhysRevApplied.3.044019.

[8] Zheng L, Lin ZH, Cheng G, Wu W, Wen X, Lee S, et al. Silicon-based hybrid cell for harvesting solar energy and raindrop electrostatic energy. Nano Energy 2014;9:291–300. https://doi.org/10.1016/j.nanoen.2014.07.024.

[9] Zheng L, Cheng G, Chen J, Lin L, Wang J, Liu Y, et al. A hybridized power panel to simultaneously generate electricity from sunlight, raindrops, and wind around the clock. Adv Energy Mater 2015;1501152. https://doi.org/10.1002/aenm.201501152.

[10] Jeon SB, Kim D, Yoon G-W, Yoon J-B, Choi Y-K. Self-cleaning hybrid energy harvester to generate power from raindrop and sunlight. Nano Energy 2015;12:636–45. https://doi.org/10.1016/j.nanoen.2015.01.039.

[11] Liu X, Cheng K, Cui P, Qi H, Qin H, Gu G, et al. Hybrid energy harvester with bi-functional nanowrinkled anti-reflective PDMS film for enhancing energies conversion from sunlight and raindrops. Nano Energy 2019;66:104188. https://doi.org/10.1016/j.nanoen.2019.104188.

[12] Yoo D, Park SC, Lee S, Sim JY, Song I, Choi D, et al. Biomimetic anti-reflective triboelectric nanogenerator for concurrent harvesting of solar and raindrop energies. Nano Energy 2019;57:424–31. https://doi.org/10.1016/j.nanoen.2018.12.035.

[13] Zhao L, Duan J, Liu L, Wang J, Duan Y, Vaillant-Roca L, et al. Boosting power conversion efficiency by hybrid triboelectric nanogenerator/silicon tandem solar cell toward rain energy harvesting. Nano Energy 2021;82:105773. https://doi.org/10.1016/j.nanoen.2021.105773.

[14] Liu Y, Sun N, Liu J, Wen Z, Sun X, Lee ST, et al. Integrating a silicon solar cell with a triboelectric nanogenerator via a mutual electrode for harvesting energy from sunlight and raindrops. ACS Nano 2016;12:2893–9. https://doi.org/10.1021/acsnano.8b00416.

[15] Helseth LE, Guo XD. Fluorinated ethylene propylene thin film for water droplet energy harvesting. Renew Energy 2016;99:845–51. https://doi.org/10.1016/j.renene.2016.07.077.

[16] Moon JK, Jeong J, Lee D, Pak HK. Electrical power generation by mechanically modulating electrical double layers. Nat Commun 2013;4:1487. https://doi.org/10.1038/ncomms2485.

[17] Lin ZH, Cheng G, Lee S, Pradel KC, Wang ZL. Harvesting water drop energy by sequential contact electrification and electrostatic induction process. Adv Mater 2014;26:4690–6. https://doi.org/10.1002/adma.201400373.

[18] Jiang D, Xu M, Dong M, Guo F, Liu X, Chen G, et al. Water-solid triboelectric nanogenerators: An alternative means for harvesting hydropower. Renew Sustain Energy Rev 2019;115:109366. https://doi.org/10.1016/j.rser.2019.109366.

[19] Tang W, Chen BD, Wang ZL. Recent progress in power generation from water/liquid droplet interaction with solid surfaces. Adv Funct Mater 2019;29:1901069. https://doi.org/10.1002/adfm.201901069.

[20] Helseth LE, Guo XD. Contact electrification and energy harvesting using periodically contacted and squeezed water droplets. Langmuir 2015;31:3269–76. https://doi.org/10.1021/la503494c.

[21] Zhu G, Su Y, Bai P, Chen J, Jing Q, Yang W, et al. Harvesting water wave energy by asymmetric screening of electrostatic charges on a nanostructured hydrophobic thin-film surface. ACS Nano 2014;8:6031–7. https://doi.org/10.1021/nn5012732.

[22] Kwon S-H, Park J, Kim WK, Yang Y, Lee E, Han CJ, et al. An effective energy harvesting method from a natural water motion active transducer. Energy Environ Sci 2014;7:3279–83. https://doi.org/10.1039/C4EE00588K.

[23] Liang Q, Yan X, Gu Y, Zhang K, Liang M, Liang S, et al. Highly transparent triboelectric nanogenerator for harvesting water-related energy reinforced by antireflection coating. Sci Rep 2015;26:4690–6. https://doi.org/10.1038/srep09080.

[24] Xiong J, Lin MF, Wang J, Gaw SL, Parida K, Lee PS. Wearable all-fabric-based triboelectric generator for water energy harvesting. Adv Energy Mater 2017;7:1701243. https://doi.org/10.1002/aenm.201701243.

[25] Lai YC, Hsiao YC, Wu HM, Wang ZL. Waterproof fabric-based, multifunctional triboelectric nanogenerator for universally harvesting energy from raindrops, wind, and human motions and as self-powered sensors. Adv Sci 2019;6:1801883. https://doi.org/10.1002/advs.201801883.

[26] Helseth LE. Electrical energy harvesting from water droplets passing a hydrophobic polymer with a metal film on its back side. J Electrostatics 2016;81:64–70. https://doi.org/10.1016/j.elstat.2016.03.006.

[27] Helseth LE. Influence of salt concentration on charge transfer when a water front moves across a junction between a hydrophobic dielectric and a metal electrode. Langmuir 2020;36:8002–8. https://doi.org/10.1021/acs.langmuir.0c01358.

[28] Yang L, Wang Y, Gao Y, Zhang W, Zhao Z. Robust working mechanism of water droplet-driven triboelectric nanogenerator: Triboelectric output versus dynamic motion of water droplet. Adv Mat Interfaces 2019;6:1901547. https://doi.org/10.1002/admi.201901547.

[29] Helseth LE, Wen HZ. Evaluation of energy generation potential of rain cells. Energy 2017;119:472–82. https://doi.org/10.1016/j.energy.2016.12.097.

[30] Choi D, Lee H, Im DJ, Kang IS, Lim G, Kim DS, et al. Spontaneous electrical charging of droplets by conventional pipetting. Sci Rep 2013;3:2037. https://doi.org/10.1038/srep02037.

[31] Song Y, Xu B, Yuan Y, Xu H, Li D. Coalescence of a water drop with an air-liquid interface: Electric current generation and critical micelle concentration (CMC) sensing. ACS Appl Mater Interfaces 2019;11:16981–90. https://doi.org/10.1021/acsami.9b00365.

[32] Jiang P, Zhang L, Guo H, Chen C, Wu C, Zhang S, et al. Signal output of triboelectric nanogenerator at oil-water-solid multiphase interfaces and its application for dual-signal chemical sensing. Adv Mat 2019;31:1902793. https://doi.org/10.1002/adma.201902793.

[33] Zhang X, Yu M, Ma Z, Ouyang H, Zou Y, Zhang SL, et al. Self-powered distributed water level sensors based on liquid-solid triboelectric nanogenerators for ship draft detecting. Adv Functional Mat 2019;29:1900327. https://doi.org/10.1002/adfm.201900327.

[34] Shi Q, Wang H, Wang T, Lee CK. Self-powered liquid triboelectric microfluidic sensor for pressure sensing and finger motion monitoring applications. Nano Energy 2016;30:450–9. https://doi.org/10.1016/j.nanoen.2016.10.046.

[35] Chen G, Liu X, Li S, Dong M, Jiang D. A droplet energy harvesting and actuation system for self-powered digital microfluidics. Lab Chip 2018;18:1026–34. https://doi.org/10.1039/C7LC01259D.

[36] Su Y, Wen X, Zhu G, Yang J, Chen J, Bai P, et al. Hybrid triboelectric nanogenerator for harvesting water wave energy and as a self-powered distress signal emitter. Nano Energy 2014;9:186–95. https://doi.org/10.1016/j.nanoen.2014.07.006.

[37] Wang J, Zhang H, Xie X, Gao M, Yang W, Lin Y. Water energy harvesting and self-powered visible light communication based on triboelectric nanogenerator. Energy Technol 2018;6:1929–34. https://doi.org/10.1002/ente.201800035.

[38] Wang J, Wang H, Li X, Zi Y. Self-powered electrowetting optical switch driven by a triboelectric nanogenerator for wireless sensing. Nano Energy 2019;66:104140. https://doi.org/10.1016/j.nanoen.2019.104140.

[39] Wijewardhana KR, Shen TZ, Song JK. Energy harvesting using air bubbles on hydrophobic surfaces containing embedded charges. Appl Energy 2017;206:432–8. https://doi.org/10.1016/j.apenergy.2017.08.211.

[40] Nguyen QT, Ahn KK. Fluid-based triboelectric nanogenerators: A review of current status and applications. Int J Precision Eng Manuf-Green Technol 2021. https://doi.org/10.1007/s40684-020-00255-x.

[41] Vo CP, Shahriar M, Le CD, Ahn KK. Mechanically active transducing element based on solid-liquid triboelectric nanogenerator for self-powered sensing. Int J Precision

Eng Manuf-Green Technol 2019;6:741–9. https://doi.org/10.1007/s40684-019-00143-z.
[42] Chen C, Wen Z, Wei A, Xie X, Zhai N, Wei X, et al. Self-powered on-line ion concentration monitor in water transportation driven by triboelectric nanogenerator. Nano Energy 2019;62:442–8. https://doi.org/10.1016/j.nanoen.2019.05.029.
[43] Zhang W, Wang P, Sun K, Wang C, Diao D. Intelligently detection and identifying liquids leakage combining triboelectric nanogenerator based self-powered sensor with machine learning. Nano Energy 2019;56:277–85. https://doi.org/10.1016/j.nanoen.2018.11.058.
[44] Helseth LE. A water droplet-powered sensor based on charge transfer to a flow-through front surface electrode. Nano Energy 2020;73:104809. https://doi.org/10.1016/j.nanoen.2020.104809.
[45] Chen C, Xie G, Yao M, Pan H, Su Y. A membrane raindrop generator and its application as a self-powered pH sensor. Micro Nano Lett 2021;16:51–7. https://doi.org/10.1049/mna2.12008.
[46] Niu J, Xu W, Tay K, He G, Huang Z, Wang Q. Triboelectric energy harvesting of the superhydrophobic coating from dropping water. Polymers 1936;2020:12. https://doi.org/10.3390/polym12091936.
[47] Neo RG, Khoo BC. Towards a larger scale energy harvesting from falling water droplets with an improved electrode configuration. Appl Energy 2021;285:116428. https://doi.org/10.1016/j.apenergy.2020.116428.
[48] Lee JW, Hwang W. Theoretical study of micro/nano roughness effect on water-solid triboelectrification with experimental approach. Nano Energy 2018;52:315–22. https://doi.org/10.1016/j.nanoen.2018.08.008.
[49] Helseth LE. The influence of microscale surface roughness on water-droplet contact electrification. Langmuir 2019;35:8268–75. https://doi.org/10.1021/acs.langmuir.9b00988.
[50] Su Y, Wang J, Wang B, Yang T, Yang B, Xie G, et al. Alveolus-inspired active membrane sensors for self-powered wearable chemical sensing and breath analysis. ACS Nano 2020;14:6067–75. https://doi.org/10.1021/acsnano.0c01804.
[51] Su Y, Yang T, Zhao X, Cai Z, Chen G, Yao M, et al. A wireless energy transmission enable wearable active acetone biosensor for non-invasive prediabetes diagnosis. Nano Energy 2020;74:104941. https://doi.org/10.1016/j.nanoen.2020.104941.
[52] Han J, Yu B, Qu G, Chen H, Su Z, Shi M, et al. Electrification based devices with encapsulated liquid for energy harvesting, multifunctional sensing, and self-powered visualized detection. J Mater Chem A 2015;3:7382–8. https://doi.org/10.1039/C4TA06168C.
[53] Choi D, Lee S, Park SM, Cho H, Hwang W, Kim DS. Energy harvesting model of moving water inside a tubular system and its application of a stick-type compact triboelectric nanogenerator. Nano Res 2015;3:7382–8. https://doi.org/10.1007/s12274-015-0756-4.
[54] Khandelwal G, Chandrasekhar A, Raj NPMJ, Kim SJ. Metal-organic framework: A novel material for triboelectric nanogenerator-based self-powered sensors and systems. Adv Energy Mater 2019;9:1803581. https://doi.org/10.1002/aenm.201803581.
[55] Salauddin Md, Rana SMS, Sharifuzzaman Md, Rahman MT, Park C, Cho H, et al. A novel MXene/Ecoflex nanocomposite-coated fabric as a highly negative and stable friction layer for high-output triboelectric nanogenerators. Adv Energy Mater 2021;11:2002832. https://doi.org/10.1002/aenm.202002832.
[56] Khandelwal G, Chandrasekhar A, Alluri NR, Vivekananthan V, Raj NPMJ, Kim SJ. Trash to energy: A facile, robust and cheap approach for mitigating environment pollutant using household triboelectric nanogenerator. Appl Energy 2018;219:338–49. https://doi.org/10.1016/j.apenergy.2018.03.031.
[57] Sun Y, Huang X, Soh S. Using the gravitational energy of water to generate power by separation of charge at interfaces. Chem Sci 2015;6:3347–53. https://doi.org/10.1039/C5SC00473J.
[58] Helseth LE, Guo XD. Hydrophobic polymer covered by a grating electrode for converting the mechanical energy of water droplets into electrical energy. Smart Mat Struct 2016;25:045007. https://doi.org/10.1088/0964-1726/25/4/045007.
[59] Liu L, Shi Q, Ho JS, Lee CK. Study of thin film blue energy harvester based on triboelectric nanogenerator and seashore IoT applications. Nano Energy 2019;66:104167. https://doi.org/10.1016/j.nanoen.2019.104167.
[60] Cho H, Chung J, Shin G, Sim JY, Kim DS, Lee S, et al. Toward sustainable output generation of liquid-solid contact triboelectric nanogenerators: The role of hierarchical structures. Nano Energy 2019;56:56–64. https://doi.org/10.1016/j.nanoen.2018.11.039.
[61] Chung J, Heo D, Kim B, Lee S. Superhydrophobic water-solid contact triboelectric generator by simple spray-on fabrication method. Micromachines 2018;9:593. https://doi.org/10.3390/mi9110593.
[62] Lee JW, Kim SM, Kim TY, Khan U, Kim SW. Water droplet-driven triboelectric nanogenerator with superhydrophobic surfaces. Nano Energy 2019;58:579–84. https://doi.org/10.1016/j.nanoen.2019.01.078.
[63] Shahzad A, Wijewardhana KR, Song JK. Contact electrification efficiency dependence on surface energy at the water-solid interface. Appl Phys Lett 2018;113:023901. https://doi.org/10.1063/1.5038605.
[64] Yu J, Ma E, Ma T. Harvesting energy from low-frequency excitations through alternate contacts between water and two dielectric materials. Sci Rep 2017;7:17145. https://doi.org/10.1038/s41598-017-17522-8.
[65] Pao YP, Yu CC, Lin YZ, Chatterjee S, Saha S, Tiwari N, et al. Carbohydrate-protein interactions studied by solid-liquid contact electrification and its use for label-free bacterial detection. Nano Energy 2021;85:106008. https://doi.org/10.1016/j.nanoen.2021.106008.
[66] Negara KMT, Wardana ING, Widhiyanuriyawan D, Hamidi N. Role of the slope on Taro leaf surface to produce electrical energy. IOP Conf Ser Mater Sci Eng 2019;494:012084. https://doi.org/10.1088/1757-899X/494/1/012084.
[67] Rasel MSU, Park JY. A sandpaper assisted micro-structured polydimethylsiloxane fabrication for human skin based triboelectric energy harvesting application. Appl Energy 2017;206:150–8. https://doi.org/10.1016/j.apenergy.2017.07.109.
[68] Parvez AN, Rahaman MH, Kim HC, Ahn KK. Optimization of triboelectric energy harvesting from falling water droplet onto wrinkled polydimethylsiloxane-reduced graphene oxide nanocomposite surface. Compos B Eng 2019;174:106923. https://doi.org/10.1016/j.compositesb.2019.106923.
[69] Wijewardhana KR, Shen TZ, Jayaweera EN, Shahzad A, Song JK. Hybrid nanogenerator and enhancement of water-solid contact electrification using triboelectric charge supplier. Nano Energy 2018;52:402–7. https://doi.org/10.1016/j.nanoen.2018.08.016.
[70] Jang S, La M, Cho S, Yun Y, Choi JH, Ra Y, et al. Monocharged electret-based liquid-solid interacting triboelectric nanogenerator for its boosted electrical output performance. Nano Energy 2020;70:104541. https://doi.org/10.1016/j.nanoen.2020.104541.
[71] Liu Y, Zheng Y, Li T, Wang D, Zhou F. Water-solid triboelectrification with self-repairable surfaces for water-flow energy harvesting. Nano Energy 2019;61:454–61. https://doi.org/10.1016/j.nanoen.2019.05.007.
[72] Xu W, Zhou X, Hao C, Zheng H, Liu Y, Yan X, et al. SLIPS-TENG: robust triboelectric nanogenerator with optical and charge transparency using a slippery interface. Natl Sci Rev 2019;6:540–50. https://doi.org/10.1093/nsr/nwz025.
[73] Chung J, Cho H, Yong H, Heo D, Rim YS, Lee S. Versatile surface for solid-solid/liquid solid triboelectric nanogenerator based on fluorocarbon liquid infuse surfaces. Sci Technol Adv Mater 2021;21:139–46. https://doi.org/10.1080/14686996.2020.1733920.
[74] Xu W, Zheng H, Zhou X, Zhang C, Song Y, Deng X, et al. A droplet-based electricity generator with high instantaneous power density. Nature 2020;578:392–6. https://doi.org/10.1038/s41586-020-1985-6.
[75] Wu H, Mendel N, van der Ham S, Shui L, Zhu G, Mugele F. Charge trapping-based electricity generator (CTEG): An ultrarobust and high efficiency nanogenerator for energy harvesting from water droplets. Adv Mater 2020;32:2001699. https://doi.org/10.1002/adma.202001699.
[76] Zhang N, Gu H, Lu K, Ye S, Xu W, Zheng H, et al. A universal single electrode droplet-based electricity generator (SE-DEG) for water kinetic energy harvesting. Nano Energy 2020;82:105735. https://doi.org/10.1016/j.nanoen.2020.105735.
[77] Zhang N, Gu H, Zheng H, Ye S, Kang L, Huang C, et al. Boosting the output performance of volume effect electricity generator (VEEG) with water column. Nano Energy 2020;73:104748. https://doi.org/10.1016/j.nanoen.2020.104748.
[78] Wu H, Chen Z, Xu G, Xu J, Wang Z, Zi Y. Fully biodegradable water droplet energy harvester based on leaves of living plants. ACS Appl Mater Interfaces 2020;12:56060–7. https://doi.org/10.1021/acsami.0c17601.
[79] Sogandares FM, Fry ES. Absorption spectrum (340–640 nm) of pure water. I. Photothermal measurements. Appl Opt 1997;36:8699–709. https://doi.org/10.1364/AO.36.008699.
[80] Marshall JS, Palmer WMK. The distribution of rainsdrops with size. J Meteorol 1948;5:165–6.
[81] Shin SS, Park SD, Choi BK. Universal power law for relationship between kinetic energy and rainfall. Adv Meteorol 2016;2016:2494681. https://doi.org/10.1155/2016/2494681.
[82] Bogan RAJ, Ohde S, Arakaki T, Mori I, McLeod CW. Changes in rainwater pH assosicated with increasing atmospheric carbon dioxide after the industrial revolution. Water Air Soil Pollut 2009;196:263–71. https://doi.org/10.1007/s11270-008-9774-0.
[83] Salve PR, Maurya A, Wate SR, Devotta S. Chemical composition of major ions in rainwater. Bul Environ Contam Toxicol 2008;80:242–6. https://doi.org/10.1007/s00128-007-9353-x.